SEGMENTATION OF SERIAL MRI OF TBI PATIENTS USING PERSONALIZED ATLAS CONSTRUCTION AND TOPOLOGICAL CHANGE ESTIMATION

Bo Wang[†,‡], *Marcel Prastawa*[†,‡], *Suyash P. Awate*[†,‡], *Andrei Irimia*[§], *Micah C. Chambers*[§],

Paul M. Vespa[♮], *John D. van Horn*[§], *Guido Gerig*[†,‡*]

[†] Scientific Computing and Imaging Institute,
[‡] School of Computing,
University of Utah

[§] Laboratory of Neuro Imaging,
[♮] Brain Injury Research Center,
University of California at Los Angeles

ABSTRACT

Traumatic brain injury (TBI) due to falls, car accidents, and warfare affects millions of people annually. Determining personalized therapy and assessment of treatment efficacy can substantially benefit from longitudinal (4D) magnetic resonance imaging (MRI). In this paper, we propose a method for segmenting longitudinal brain MR images with TBI using personalized atlas construction. Longitudinal images with TBI typically present topological changes over time due to the effect of the impact force on tissue, skull, and blood vessels and the recovery process. We address this issue by defining a novel atlas construction scheme that explicitly models the effect of topological changes. Our method automatically estimates the probability of topological changes jointly with the personalized atlas. We demonstrate the effectiveness of this approach on MR images with TBI that also have been segmented by human raters, where our method that integrates 4D information yields improved validation measures compared to temporally independent segmentations.

Index Terms— 4D pathology segmentation, longitudinal MRI, topological change estimation, atlas construction.

1. INTRODUCTION

Improved therapy in traumatic brain injury (TBI) is an important driving biological problem for the medical community as TBI is a major cause of death and disability worldwide, especially in children and young adults. It is a significant problem in health care as it affects about 1.7 million people in the United States every year [1]. Robust, reproducible segmentations of longitudinal magnetic resonance (MR) images with TBI are crucial for quantitative analysis of pathology and of recovery to measure treatment efficacy. A challenging problem for longitudinal segmentation of TBI images is the change of brain structure due to lesions (primarily swelling/edema and bleeding). At different time points

and stages, lesions may deform and they can also disappear or appear due to intervention, recovery or formation of new injuries. Thus, 4D segmentation methods for TBI need to be able to map images over time and handle topological changes.

Longitudinal segmentation algorithms [2, 3] use information from all time points to achieve optimal results. This requires registration of each image to a reference time point or an atlas. Many image registration methods assume that there are no topological changes between images and use diffeomorphic (smooth and invertible) mappings. However, for longitudinal images with TBI this assumption no longer holds and it is necessary to model topological changes (Fig. 1).
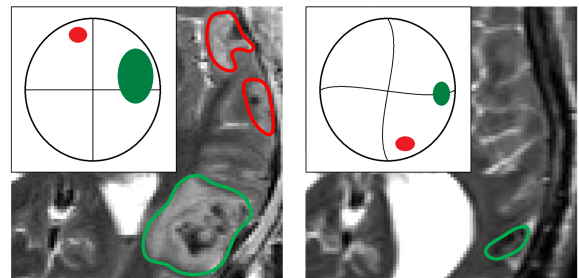

Fig. 1. Illustration of topological changes in longitudinal MR images with TBI. Left is the acute baseline T2 image, right the chronic followup T2 image, each overlaid with a sketch mock figure. Red indicates lesions with topological changes over time (either disappearing or appearing lesions). Green indicates lesions that deform without topological changes.

Several researchers have proposed methods [4, 5, 6, 7, 8] for registering images with topological changes due to missing or newly appearing structures. Periaswamy and Farid proposed a registration method for images with missing correspondence in which topological changes were detected through difference of image intensities [4]. Li et al. proposed a registration method using Riemannian embedding that accounts for deformation and intensity changes [5]. Chitphakdithai and Duncan proposed a postresection intensity prior for alignment of preoperative and postresection

brain images [6]. Niethammer et al. proposed a registration method for TBI images using geometric metamorphosis that maps known lesion boundaries over time [7]. Ou et al. proposed a generic deformable registration method using attribute matching and mutual-saliency weighting [8]. These image registration methods do not provide anatomical information unlike segmentation and atlas construction methods.

In this paper, we propose a longitudinal segmentation method that relies on personalized atlas construction and topological change estimation. The method iteratively estimates the image appearance model and the spatial anatomical model that undergoes diffeomorphic deformation and non-diffeomorphc/topological changes. We define a novel objective function for personalized atlas construction with topological changes. This objective function gives rise to joint estimation of anatomical priors, diffeomorphic mappings, and the probability of topological changes for a longitudinal MR image sequence.

2. METHOD

2.1. Estimation of Image Appearance Model

Given multimodal images at time point t denoted by $I^t = \{I(x_1), \ldots, I(x_N)\}^t$ with N voxels indexed by positions x and M_t number of channels, we use mixtures of Gaussians to model the data following van Leemput et al. [9]. We estimate the Gaussian mixture parameters that maximizes the log likelihood function for each time point t:

$$\sum_x \log \sum_{c=1}^{C^t} p(I^t(x)|\mu_c^t, \Sigma_c^t)\Pi_c^t(x) \quad (1)$$

where $p(I^t(x)|\mu_c^t, \Sigma_c^t)$ is the multivariate Gaussian probability distribution with mean μ_c^t and covariance Σ_c^t, C^t is the number of classes at time point t, and Π_c^t is the spatial prior for class c at time t.

The number of classes C^t at different time points in longitudinal images with TBI typically varies because hemorrhagic lesions (bleeding) and non-hemorrhagic lesions (swelling / edema) may disappear in follow-up scans due to recovery. We address the problem of mapping variable numbers of lesion classes by combining the posteriors of lesion classes (bleeding and edema) into one. The combination of lesion posteriors yields a unified class posterior for all lesions and thus gives us equal number of classes C for the posteriors $P_c^t = \frac{p(I^t|\mu_c^t, \Sigma_c^t)\Pi_c^t}{\sum_{c'} p(I^t|\mu_{c'}^t, \Sigma_{c'}^t)\Pi_{c'}^t}$ at each time point t that is used to construct personalized atlases.

2.2. Personalized Atlas Construction

We use the posteriors $P^t = \{P_{c=1}^t \cdots P_{c=C}^t\}$ to build a personalized atlas A^t at each time point t. We smoothly subdivide the image into diffeomorphic and non-diffeomorphic
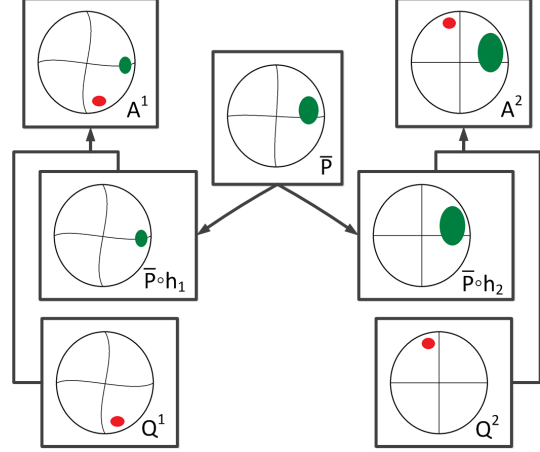

Fig. 2. Construction of a personalized spatiotemporal atlas using diffeomorphic and non-diffeomorphic components. The diffeomorphic component is the temporally global atlas $\bar{P}$ that is mapped to each time point while preserving topology of $\bar{P}$. The non-diffeomorphic components are the temporally local pdfs Q_t at each time point t that may change the topology between different time points. Regions that change diffeomorphically are colored in green, while regions that change topology are colored in red.

regions using the probability of topological change denoted by $\Gamma^t \in [0, 1]$. We define the personalized atlas at time point t using Γ^t as

$$A^t = (1 - \Gamma^t)\bar{P} \circ h_t + \Gamma^t Q^t. \quad (2)$$

The personalized atlas A^t is a combination of an atlas $\bar{P}$ that has been mapped using the diffeomorphic mapping h_t and a temporally specific atlas Q^t (Fig. 2). The parameters that define the personalized atlas is chosen such that the diffeomorphic component (weighted by $(1 - \Gamma^t)$) matches $\bar{P}$ to P^t, and the non-diffeomorphic component (weighted by Γ^t) matches Q^t to P^t. Thus, personalized atlas construction is formulated as a minimization of the energy function $\Psi =$

$$\sum_t \| (1 - \Gamma^t)(P^t - \bar{P} \circ h_t) \|^2 + \| \Gamma^t(P^t - Q^t) \|^2$$
$$+ w \| \Gamma^t \|^2 + R(h_t). \quad (3)$$

where $R(\cdot)$ denotes the regularization term that enforces h_t to be diffeomorphic mappings and w is the scalar weight for the regularization term for Γ^t that enforces sparsity.

We take the derivative with respect to Q^t and Γ^t and set the derivatives as zero to get the updates for Q^t and Γ^t. The temporally specific atlas Q^t is estimated from

$$\nabla_{Q^t}\Psi(x) = -2\,\Gamma^t(x)(P^t(x) - Q^t(x)) = 0, \quad (4)$$

Obtaining $Q^t = P^t$. The probability of topological change Γ^t is estimated using $\nabla_{\Gamma^t}\Psi(x) =$

$$-2\,(1 - \Gamma^t(x)) \| P^t(x) - \bar{P}^t(x) \|^2$$
$$+ 2\,\Gamma^t(x) \| P^t(x) - Q^t(x) \|^2 + 2\,w\,\Gamma^t(x). \quad (5)$$

where $\bar{P}^t$ is $\bar{P} \circ h_t$. Setting $\nabla_{\Gamma^t} \Psi(x) = 0$, we get

$$\Gamma^t(x) = \frac{\| P^t(x) - \bar{P}^t(x) \|^2}{\| P^t(x) - \bar{P}^t(x) \|^2 + w}. \quad (6)$$

The intuition for Γ^t update is that when correspondence exists between two time points (no topological change), the temporal difference $\| P^t(x) - \bar{P}^t(x) \|^2$ is small, so $\Gamma^t(x) \to 0$; when there is no correspondence, the temporal difference is large, so $\Gamma^t(x) \to 1/(1+w)$. Our topological change estimation Γ^t based on optimization of Ψ provides a justification for the weight function in [4]. The estimation of the diffeomorphic atlas $\bar{P}$ and the diffeomorphic mapping h_t yields a method identical to standard computational anatomy algorithms [10], where we use modified gradient equations concerning the diffeomorphic component.

2.3. Segmentation Algorithm

The segmentation algorithm that combines the estimation of the image appearance model and the construction of personalized atlas is presented below. We use user input that indicates the areas showing major lesions and lesion types as spheres to initialize the algorithm. These spheres function as rough estimates of the segmentations that will be refined by our algorithm by adding or removing lesions as necessary.

$P^t \leftarrow$ temporally independent segmentation with user input
$\Gamma^t \leftarrow 0.5$
Repeat until convergence
    $\bar{P}^t \leftarrow \bar{P}^t - \epsilon \nabla_{\bar{P}^t} \Psi$
    $h^t \leftarrow h^t - \epsilon \nabla_{h^t} \Psi$
    $Q^t \leftarrow P^t$
    Update Γ^t using Equ. (6)
    $A^t \leftarrow (1 - \Gamma^t)\bar{P} \circ h_t + \Gamma^t Q^t$
    $P^t \leftarrow$ segmentation using prior $\Pi^t = A^t$

---

3. RESULTS AND VALIDATION

We apply our framework to multimodal image data of three subjects with TBI. Each subject was scanned at two time points: acute scan at ≈ 3 days and chronic scan at ≈ 6 months. The image data of each subject include T1, T2, FLAIR, and GRE modalities. Acute and chronic images of Subject I is shown in Fig. 3 where non-hemorrhagic lesions (edema / swelling) are shown as hyperintense regions in FLAIR while hemorrhagic lesions (bleeding) are shown as hypointense regions in T2 and GRE.

    We validate our method by comparing our results to manual segmentations by a human expert that act as ground truth. For comparison, we also show results of independent 3D segmentations at each time point. We use the Dice coefficient as our comparison measure, which measures the volumetric overlap of two binary segmentations and lies in $[0, 1]$. Table 1
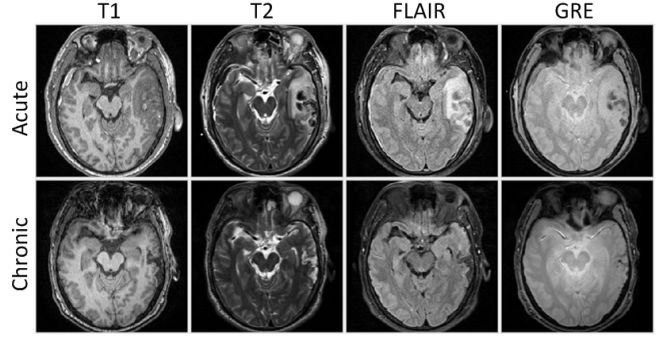

Fig. 3. Axial views of acute and chronic images of Subject I.

Lesion types	Subject	Dice values		
		ANHL	AHL	CL
Indepedent analysis	I	0.5311	0.5135	0.2576
	II	0.2444	0.5107	0.1367
	III	0.4747	0.2940	0.1963
Joint analysis	I	0.6069	0.5683	0.3383
	II	0.5009	0.5194	0.5578
	III	0.6563	0.3557	0.1999

Table 1. Dice values comparing semi-automatic segmentation to ground truth, using temporally independent segmentations and our approach. AHL and ANHL are acute hemorrhagic and non-hemorrhagic lesions, CL is chronic lesion.
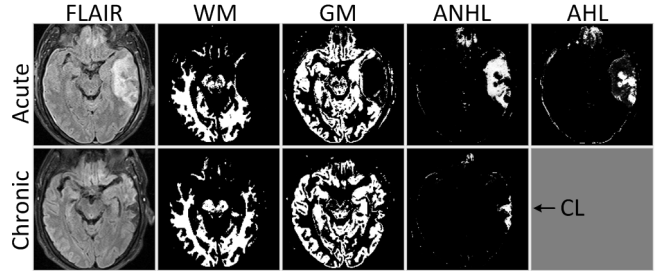

Fig. 4. Segmentations of our method for acute images of Subject I. AHL and ANHL are acute hemorrhagic and non-hemorrhagic lesions (edema), CL is chronic lesion (necrosis).

shows the comparisons of both methods against the ground truth. In this experiment, initial Γ^t is 0.5 and w is 1.0. The Dice coefficient values are relatively low due to the complex shapes of the small lesions, but important are the differences between independent and joint analysis of the two time points.

    Coronal view of the final posteriors of subject I using our framework are shown in Fig. 4. The evolving posteriors P^t of subject I are shown in Fig. 5. The initial posteriors for both non-hemorrhagic and hemorrhagic lesions are suboptimal, and the posteriors are improved at each iteration of our algorithm. In particular, the initial posteriors for hemorrhagic lesions are incorrect as the user initialization covers the
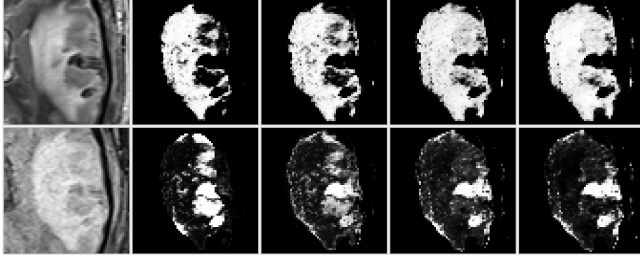
Fig. 5. The evolving posteriors P^t of the lesion classes for the acute images of Subject I. Top left is acute T2 image followed by the posteriors of non-hemorrhagic lesion from iteration 1 to 4, bottom left is acute FLAIR image followed by the posteriors of hemorrhagic lesion from iteration 1 to 4.
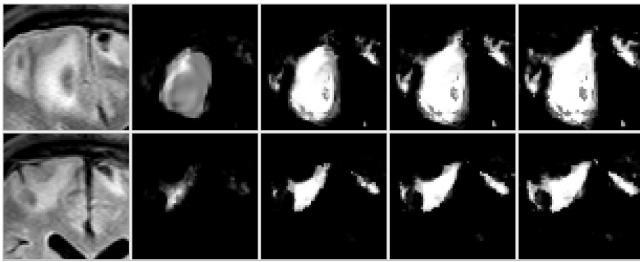

Fig. 6. The evolving personalized atlas A^t generated by our method for the acute ($t = 1$) and chronic ($t = 2$) images of Subject II. Top left is acute FLAIR image followed by the A^1 from iteration 1 to 4, bottom left is chronic FLAIR image followed by the A^2 from iteration 1 to 4.

boundary between lesion and white matter. However, the final posteriors of hemorrhagic lesions provides segmentation that matches the observed image data. Fig. 6 shows the evolving personalized atlas A^t of lesion class of subject II. A^t changes gradually to match P^t because we estimate personalized atlases that are similar to the segmentations at each time point.

4. CONCLUSIONS

We have presented a segmentation method for longitudinal MR images of TBI patients that uses personalized atlas construction and topological change estimation. Our method combines 4D information through the creation of personalized atlas that explicitly handles diffeomorphic and nondiffeomorphic temporal changes. The method is robust to topological changes caused by the injury and the recovery process in TBI. We have shown that the method provides improved results compared to temporally independent analysis which ignores temporal relationships.

Our proposed approach relies on user input to localize samples of various lesion types. In the future, we plan to automate this process using prior knowledge on the appearance of lesions in different MR modalities. The method generates complete 4D segmentations of healthy structures as well as lesions which has potential for quantifying changes over time due to recovery under individually chosen treatment. Automated segmentation and quantitative analysis of longitudinal changes of brain tissue and lesions may give clinicians the highly valuable information about future improved treatment and therapeutic interventions for TBI patients.

5. REFERENCES

[1] M. Faul, L. Xu, M.M. Wald, and V.G. Coronado, *Traumatic brain injury in the United States: Emergency department visits, hospitalizations and deaths 2002-2006*, Atlanta (GA): Centers for Disease Control and Prevention, National Center for Injury Prevention and Control; 2010.

[2] T. Riklin-Raviv, K. Van Leemput, B.H. Menze, W.M. Wells, and P. Golland, "Segmentation of image ensembles via latent atlases," *Medical Image Analysis*, vol. 14, no. 5, pp. 654–665, 2010.

[3] B. Wang, M. Prastawa, A. Irimia, M. C. Chambers, P. M. Vespa, J. D. Van Horn, and G. Gerig, "A patient-specific segmentation framework for longitudinal MR images of traumatic brain injury," *Proc. SPIE*, 8314, 831402 (2012).

[4] S. Periaswamy and H. Farid, "Medical image registration with partial data," *Medical Image Analysis*, vol. 10, no. 3, pp. 452–464, 2006.

[5] X. Li, X. Long, and C. Wyatt, "Registration of images with topological change via Riemannian embedding," in *IEEE ISBI*, 2011, pp. 1247–1252.

[6] N. Chitphakdithai and J. S. Duncan, "Non-rigid registration with missing correspondences in preoperative and postresection brain images," in *MICCAI (1)*, 2010, pp. 367–374.

[7] M. Niethammer, G. L. Hart, D. F. Pace, P. M. Vespa, A. Irimia, J. D. Van Horn, and S. R. Aylward, "Geometric metamorphosis," in *MICCAI (2)*, 2011, pp. 639–646.

[8] Y. Ou, A. Sotiras, N. Paragios, and C. Davatzikos, "DRAMMS: Deformable registration via attribute matching and mutual-saliency weighting," *Medical Image Analysis*, vol. 15, no. 4, pp. 622–639, 2011.

[9] K. Van Leemput, F. Maes, D. Vandermeulen, and P. Suetens, "Automated model-based tissue classification of MR images of the brain," *IEEE TMI*, pp. 897–908, 1999.

[10] L. Younes, F. Arrate, and M. I. Miller, "Evolutions equations in computational anatomy," *NeuroImage*, vol. 45, no. 1, pp. S40 – S50, 2009.